ELSEVIER

Wear 250 (2001) 593–603

WEAR

www.elsevier.com/locate/wear

Wear of the blade diamond tools in truing vitreous bond grinding wheels Part II. Truing and grinding forces and wear mechanism

Albert J. Shih [a,*], William I. Clark [a], Jeffrey L. Akemon [b]

[a] *Department of Mechanical and Aerospace Engineering, North Carolina State University, Raleigh, NC 27695-7910, USA*
[b] *Cummins Engine Company, Columbus, IN 47202-3005, USA*

Abstract

Truing and grinding forces and the wear mechanism of particle and rod diamond blade tools used to generate precise and intricate forms on rotating vitreous bond silicon carbide grinding wheels are presented. A Hall effect sensor was used to measure the change of grinding spindle power during truing and grinding. A signal processing procedure was developed to identify individual truing passes and to extract the average, peak-to-valley, and standard deviation of the variation of truing force for each pass. The truing force data and SEM micrographs of worn surfaces on blade tools reveal micro- and macro-fracturing of the diamond. The attritious and erosion wear of the diamond rod and particle, erosion of the metal bond, and pulling-out of the diamond particle are also identified. Grinding force data shows that, for the same truing parameters, a wheel trued by the rod diamond blade tool has higher grinding forces than one trued by a particle diamond blade tool.

Keywords: Diamond wear; Truing force; Ceramic grinding

1. Introduction

The truing and grinding forces and scanning electron microscopy (SEM) micrographs of the rod and particle diamond on the blade tools for truing vitreous bond SiC grinding wheels are presented. The slow and steady wear of diamond tools is the key to achieving consistent wheel surface conditions and reliable grinding results. Experimental observations in this and previous studies showed the wear of diamond grit or rod during truing is not a steady process.

The wear of diamond particles on the grinding wheel has been studied by Webb and Jackson [1], Liao and Luo [2], Luo [3], and Wright and Wapler [4]. Miller and Ball [5] analyzed the wear of diamonds in impregnated diamond bit drilling. Werner and Minke [6] investigated the wear of polycrystalline diamond as the tool for dressing conventional grinding wheels. These researches reveal the types of wear of diamond, such as the micro-fractured, macro-fractured, polished (flattened), and pulled-out diamond grits, and the erosion of the bond material supporting the diamond. The same analysis method is applied to study the wear of diamond rods and particles on the blade tool.

Consider a diamond particle in the front of the particle diamond blade tool. The metal bond between this diamond particle and grinding wheel is gradually ground away. This exposes the grinding particle to the grinding wheel. This diamond particle then acts as a cutting point to remove the abrasive and bond on the grinding wheel, a typical two-body abrasion [7]. Wear occurs on the diamond particle, which is subjected to a large force and high temperature. The wear on the diamond particle steadily increases the contact surface area and the force on the grit. At the same time, the metal bond support around the diamond grit is slowly eroded away. As the wear process reaches a critical point when the bond can no longer support the high contact force, the diamond particle is fractured or pulled-out of the tool. The debris sometimes squeezes in between the tool and the wheel, creating a sudden change in the truing force.

For the rod diamond blade tool, a similar wear process occurs. Instead of the fracture and pulling-out of diamond grits, the diamond rod fractures, exposing a sharp contact point for truing the grinding wheel. Truing force data and SEM micrographs are used to study the wear mechanism of the blade diamond tools. After truing, the SiC wheel is used to grind a zirconia workpiece to identify the effects of truing parameters on grinding.

In this paper, the measurement of truing and grinding forces is first introduced. Results of truing forces are then discussed. SEM micrographs of the worn diamond grits and rods are presented to study the wear mechanism. Finally, the effect of truing on grinding forces is analyzed.

* Corresponding author. Tel.: +1-919-515-5260; fax: +1-919-515-7968.
E-mail address: ajshih@eos.ncsu.edu (A.J. Shih).

0043-1648/01/$ – see front matter
PII: S0043-1648(01)00611-1

Table 1
Properties and dimensions of the zirconia workpiece

Workpiece material	MgO transformation toughened zirconia
Hardness (N/mm^2)	9800 (under 4.9 N load)
Average grain size (mm)	0.06
Flexural bending strength (MPa)	620–690
Density (g/cm^3)	5.6–5.8
Dimension of original blank (mm)	9.0
Diametrical material removal (mm)	5.0

2. Truing and grinding force measurement

During truing, the power change in the grinding wheel spindle was measured using a power sensor [8,9]. The level of power change in truing, ΔW_t, was converted to the tangential truing force, F_{tt}.

$$F_{tt} = \frac{\Delta W_t}{v_s} \quad (1)$$

where v_s is the surface speed of the grinding wheel. The spindle power data for the entire truing process, which may take several hours at slow truing traverse speeds, was recorded by a data-acquisition system.

After truing, the SiC wheel was used for cylindrical plunge grinding of a zirconia part to identify the effect of truing parameters on grinding forces. Properties of the zirconia work-material used in this study are listed in Table 1. The same Hall effect power sensor for the grinding wheel spindle was used to measure the peak power change, ΔW_g, at the start of the cylindrical plunge grinding process. ΔW_g was converted to the peak tangential grinding force, and the peak tangential grinding force was then divided by the width of contact in grinding, b, to calculate the peak specific tangential grinding force, f_{gt}.

$$f_{gt} = \frac{\Delta W_g}{b v_s} \quad (2)$$

b was set to 7.6 mm in this study.

3. Analysis and experimental results of the truing force

A total of 32 truing experiments were conducted on two types of diamond tools at four truing feeds and four traverse speeds. Each truing test involves a large number (about 80–90) of repetitive truing passes. Due to the immense amount of data, it is not feasible to present all the truing force results. Two representative sets of truing force data at two extreme conditions were presented for the two (rod

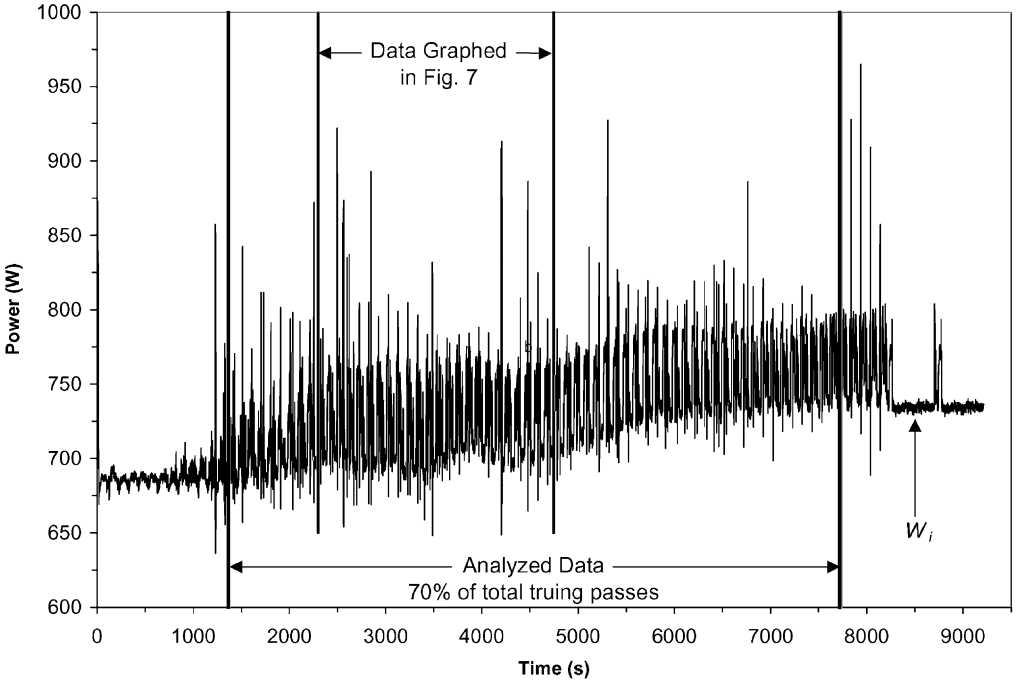

Fig. 1. Measured spindle power for truing at 1 μm feed and 13 mm/min traverse speed using the particle diamond blade tool and the drifting of W_i, the idle power loss of spindle motor.

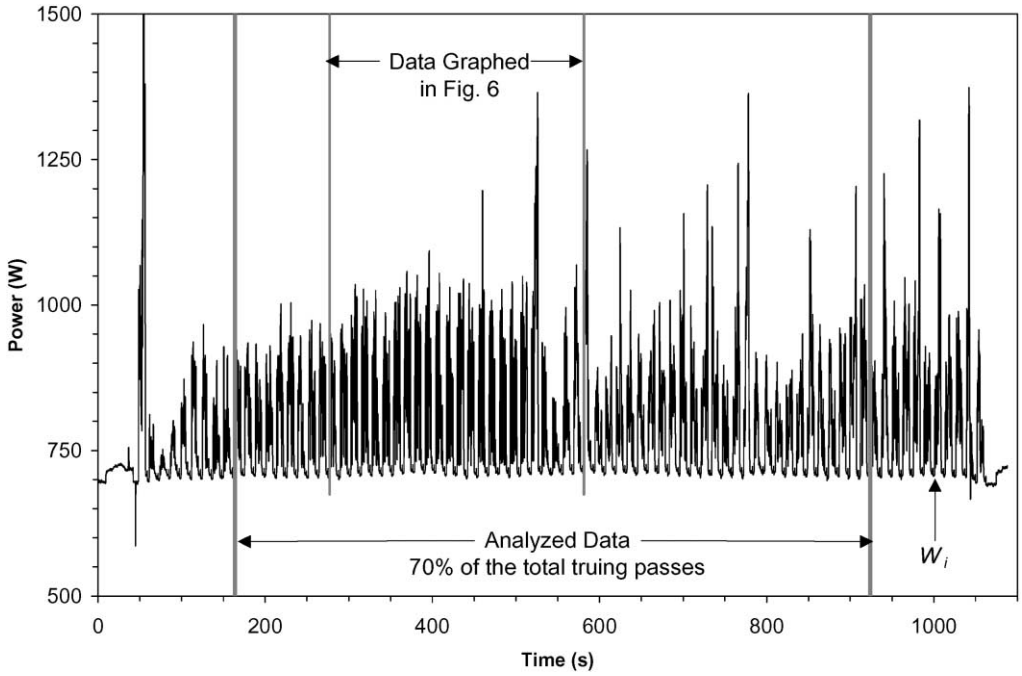

Fig. 2. Measured spindle power for truing at 10 μm feed and 125 mm/min traverse speed using the rod diamond blade tool.

and particle) diamond tools. These two extreme conditions are: (1) truing at the smallest feed (1 μm) and slowest traverse speed (13 mm/min), and (2) truing at the largest feed (10 μm) and fastest traverse speed (125 mm/min). In total, four sets of truing force data are closely examined.

Figs. 1 and 2 show the measured spindle power data for truing at 1 μm feed and 13 mm/min traverse speed using the particle diamond tool and truing at 10 μm feed and 125 mm/min traverse speed using the rod diamond tool, respectively. The sampling rate was set to collect two data points per second for the slow traverse speed (13 mm/min) and 16 data points per second for the high traverse speed (125 mm/min). Both Figs. 1 and 2 show that the inherent loss of the spindle motor power, as represented by W_i, exists. Fig. 1 also illustrates the problem of drifting W_i during the long, 2.2 h or 8000 s, truing test with slow traverse speed.

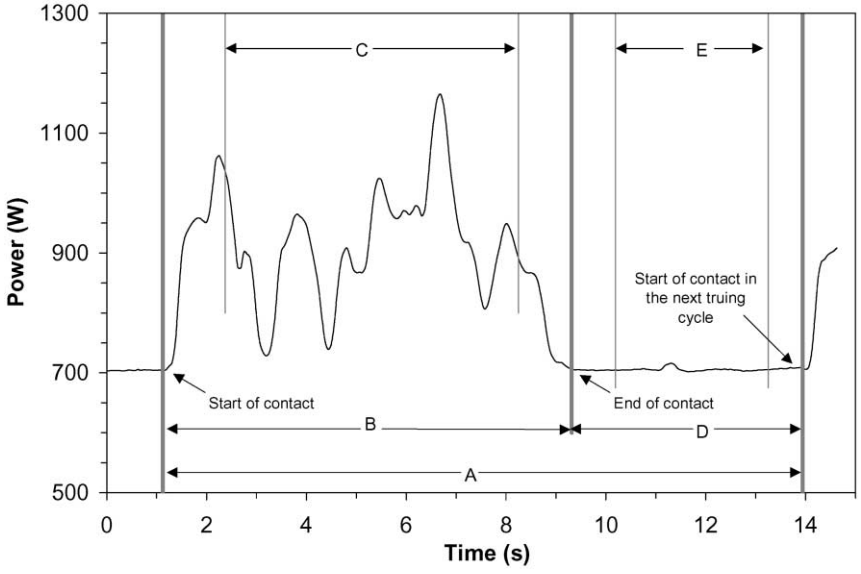

Fig. 3. Sections in the truing force trace used to calculate the datum, average, peak-to-valley, and standard deviation of truing force.

As shown in Fig. 2, this drifting problem still exists during truing with fast traverse speed, although at a less extensive magnitude.

To overcome this drifting problem, a signal processing procedure was developed to find the datum and change in power for each individual truing pass. First, the time period and the start and end of each truing pass are identified. The truing force data can then be separated into a series of individual truing passes. The signal of a typical truing pass is shown in Fig. 3. Each truing pass is further divided into five sections, A through E. Section A is the individual truing pass, which is about 100 s for the slow traverse speed (13 mm/min) and 10 s for the fast traverse speed (125 mm/min) while truing the 20 mm wide grinding wheel. The time period from start to end of the contact between the diamond tool and grinding wheel is labeled as Section B. Section D is the time when the machine is repositioning and the diamond tool is not in contact with the grinding wheel.

It is difficult to pinpoint the exact start and end of a truing cycle. Therefore, the data analysis is conducted at the middle 70% portion of Sections B and D. The datum W_i for each truing pass is calculated by averaging the data points in

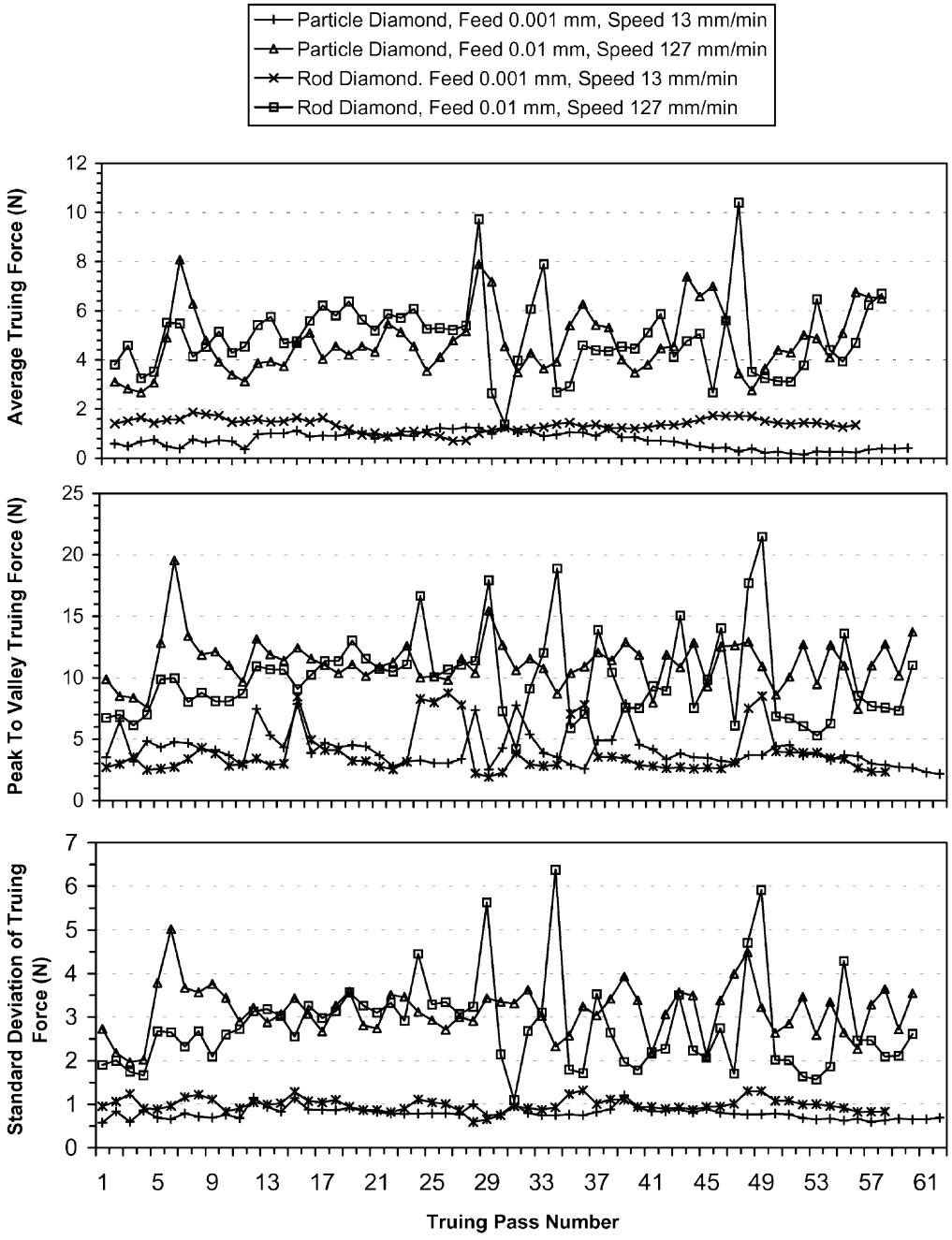

Fig. 4. Average, peak-to-valley, and standard deviation of the truing force for the four selected sets of truing force data.

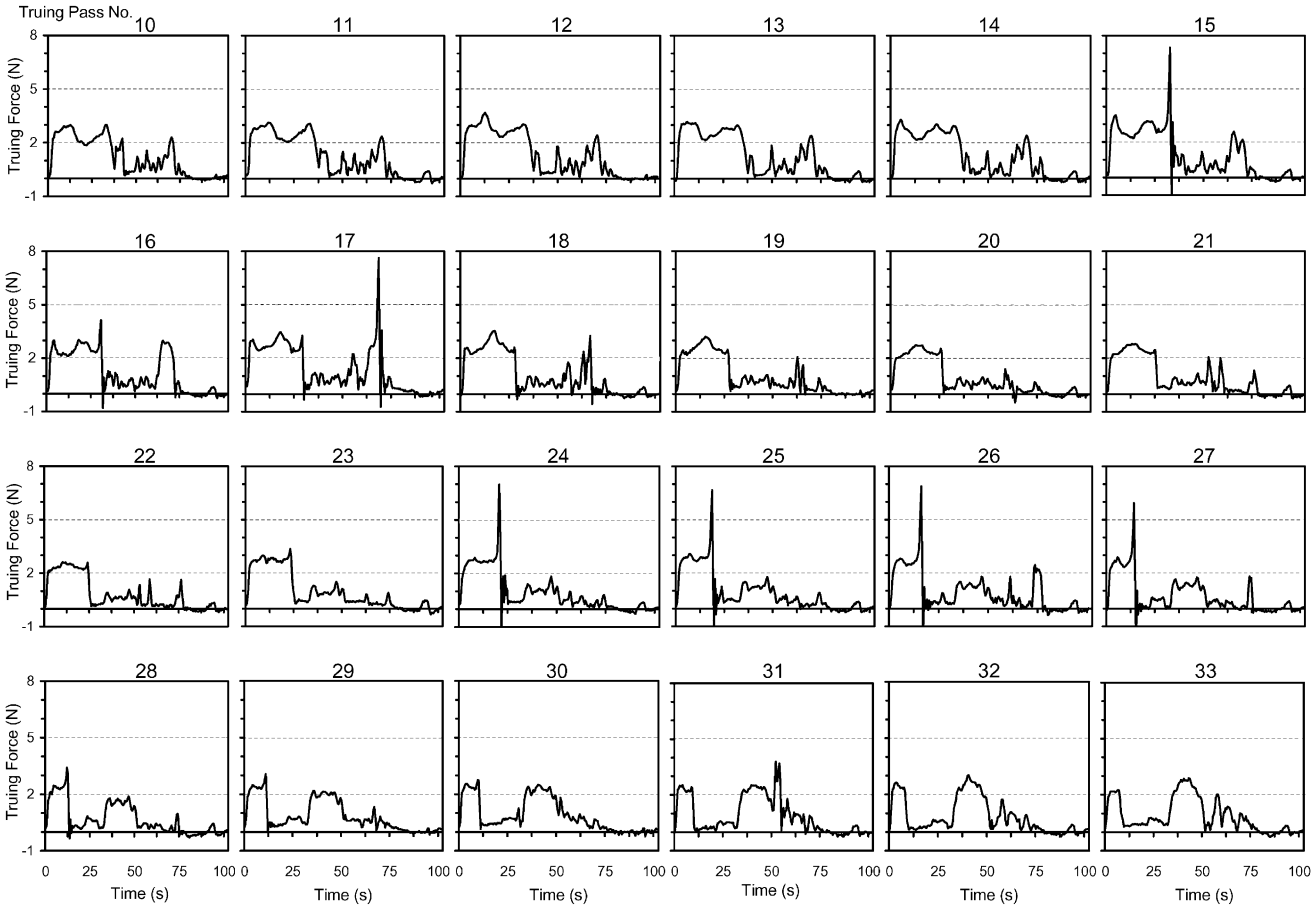

Fig. 5. Twenty-four consecutive tangential truing force data for truing at 1 μm feed and 13 mm/min traverse speed using the rod diamond blade tool.

Section E, which is 70% of the time duration in the middle of Section D. The datum is used as the base or zero to find the change in spindle power for each truing pass. The magnitude of spindle power in Section C, the middle 70% portion of Section B, relative to the datum (Section E) is the spindle power change due to truing, ΔW_t. ΔW_t is converted to the truing force using Eq. (1). Statistical analysis is used to analyze the truing force data in Section C. The average, peak-to-valley, and standard deviation of the truing force data for each truing pass are extracted.

Results of the average, peak-to-valley, and standard deviation of the truing force versus the truing pass number for the middle 70% of the four selected truing experiments are shown in Fig. 4. The first 15% of the truing force data are not analyzed to avoid possible transient results at the start of the truing. For example, for the first 10–15 truing passes, Fig. 1 shows the relatively low truing force and Fig. 2 show a spike of very high truing force in the beginning of the truing process. In Fig. 4, the first truing pass is not the first actual truing pass because the first 15% of the data set was discarded. Similarly, the last truing pass in Fig. 4 is not the actually the last truing pass of the experiment. Figs. 5–8 present the truing force versus time results for truing pass numbers 10–33 of the analyzed data (24 truing passes).

The unsteady nature of the truing force can be identified on all four sets of truing conditions. In Figs. 5–8, the truing force does suddenly drop to near zero several times in almost every truing pass. This may be caused by micro-fracturing of the diamond particle or rod. High peaks of truing force are be seen in all cases. As shown in Fig. 6, the highest truing force (23 N) occurs in truing pass #29. The level of truing force following this peak (pass #30–33) are low, which represents the possibility of diamond macro-fracturing happening at the peak force in truing pass #29 in Fig. 6.

Based on Fig. 4, effects of truing feed, traverse speed, and diamond type are concluded as follows:

- *Effect of truing feed and traverse speed*: Truing at high feed (10 μm) and traverse speed (125 mm/min) does consistently generate a higher average, peak-to-valley, and standard deviation of the truing force than the low feed (1 μm) and speed (13 mm/min) conditions.
- *Effect of diamond type*: The type of diamond tool does not appear to affect the peak-to-valley or standard deviation of the truing force, i.e. the variation of the truing force using these two types of diamond tools is about the same. For the particle diamond tool, consistently lower average

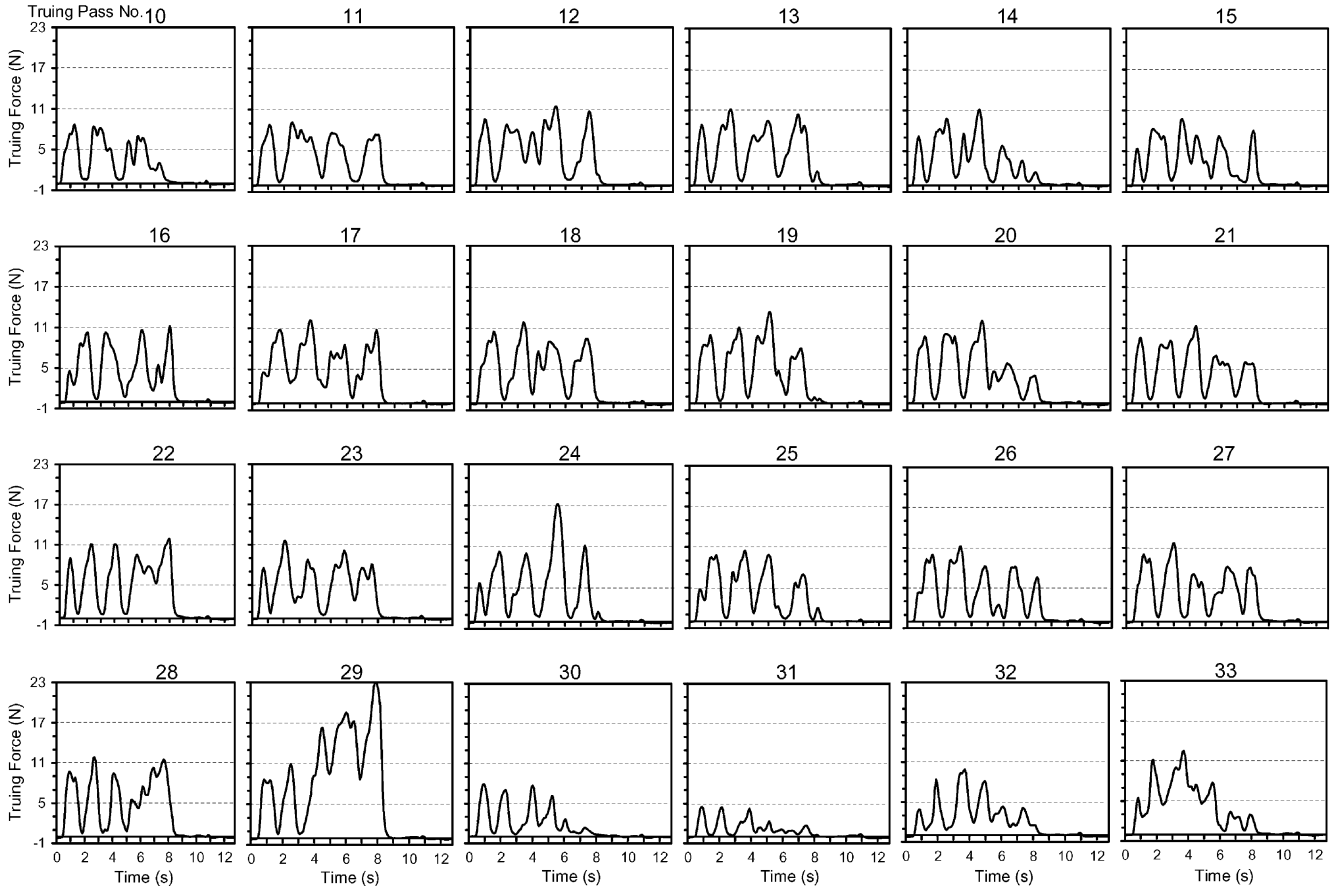

Fig. 6. Twenty-four consecutive tangential truing force data for truing at 10 μm feed and 125 mm/min traverse speed using the rod diamond blade tool.

truing forces can be seen while truing with the low truing feed and speed.

4. SEM micrographs of the blade diamond tools

The worn surfaces of the rod and particle diamond blade tools were examined using the SEM to identify the wear pattern of the diamond rods and particles. The overall views of the surfaces on rod and particle diamond blade tools are shown in Fig. 9.

4.1. Rod diamond tool

Five diamond rods can be identified on the surface of the blade tools. These diamond rods and the direction of abrasive on the grinding wheel moving across this blade diamond tool are shown in Fig. 9(a).

- *Rod diamond* #1: As shown in Fig. 9(a), the abrasive on grinding wheel needs to pass the other four diamond rods before reaching rod diamond #1. Fig. 10(a) shows that this rod diamond, originally about 0.3 mm × 0.3 mm in size, is covered by metal debris. This indicates the possibility that the diamond rod macro-fractured, generating a cavity and that metal debris fills out the cavity and partially covers the diamond rod. The track of bond erosion can also be seen in Fig. 10(a). Fig. 10(b) shows the flat worn surface on this diamond rod.
- *Rod diamond* #2: The square corner of the diamond rod and the large wear flat, due to attritious wear, of rod diamond #2 can be seen in Fig. 10(c) and (d), respectively.
- *Rod diamond* #3: The 0.3 mm × 0.3 mm square shape and erosion of metal bond around the rod diamond can clearly be seen in Fig. 10(e). Fig. 10(f) shows a close-up view of the wear flat on the corner of diamond rod #3.
- *Rod diamond* #4: Rod diamond #4 and two pieces of broken diamond fragments can be seen in Fig. 10(g). The track of bond erosion can also be identified. These two fragments are located above rod diamond #4 because the blade tool was moving across the grinding wheel, which created a side force acting on the diamond fragments after fracture. A close-up view of the wear flat on rod diamond #4 is shown in Fig. 10(h).
- *Rod diamond* #5: Fig. 10(i) shows rod diamond #5 and its broken fragments on the side. This picture demonstrates a macro-fracture of the rod diamond. Based on the direction of truing in the experiment, box E in Fig. 10(i) (close-up

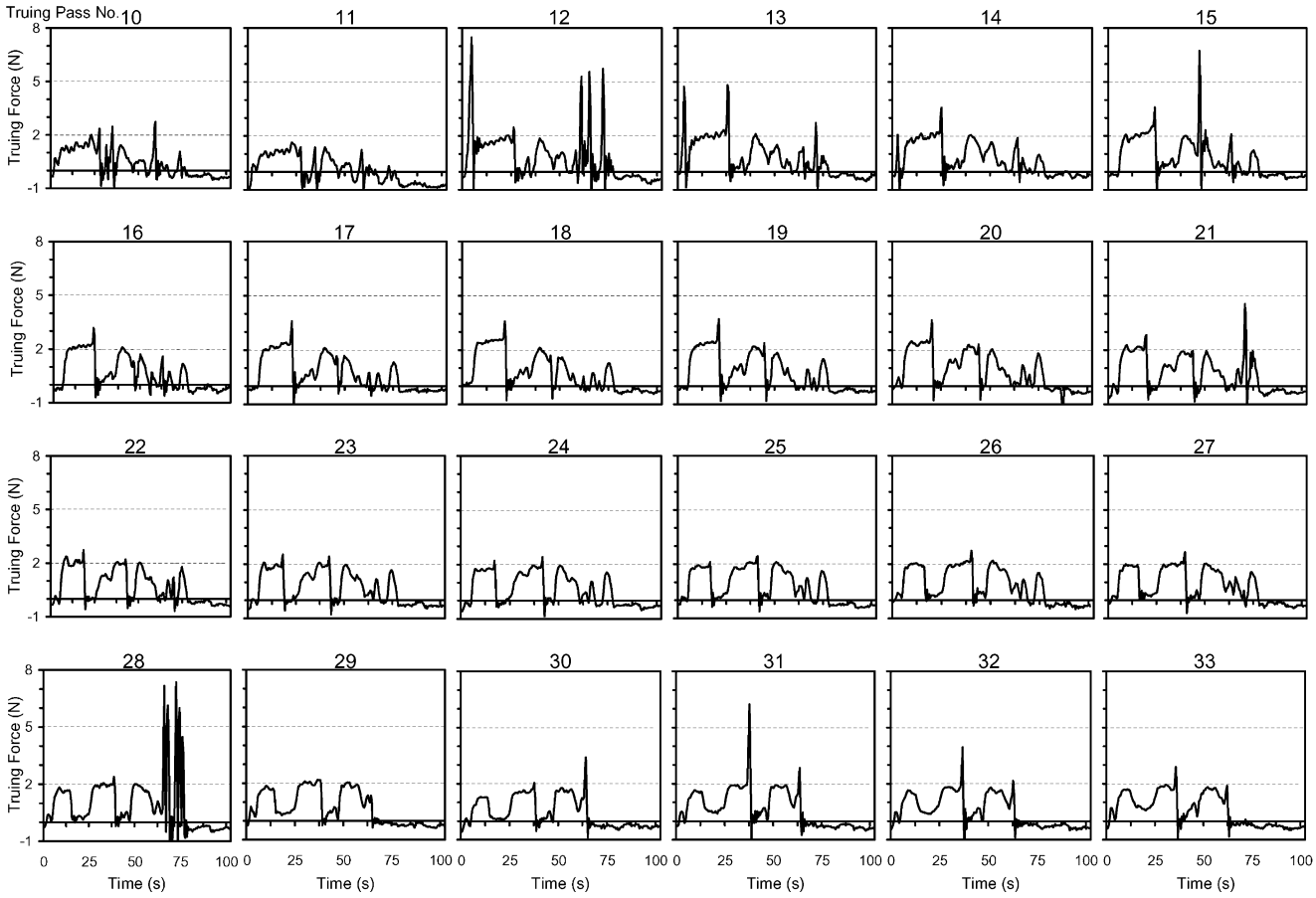

Fig. 7. Twenty-four consecutive tangential truing force data for truing at 1 μm fee and 13 mm/min traverse speed using the particle diamond blade tool.

view in Fig. 10(j)) is the original rod diamond #5, and box F in Fig. 10(i) (close-up view in Fig. 10(k)) is the diamond fragment. This diamond fragment, as shown in Fig. 10(j), does not have the wear flat, indicating that this diamond rod has not yet engaged the grinding wheel. On the contrary, the diamond fragment in box F has the attritious wear flat, as shown in Fig. 10(l).

4.2. Particle diamond tool

Five diamond grits can be observed on the surface of the blade tool. The direction of abrasive moving across this tool is indicated in Fig. 9(b).

- *Particle diamond* #1: Fig. 11(a) and (b) show particle diamond #1 and its close-up view, respectively. Erosion and micro-fracture of the diamond grit can be seen. However, this diamond does not have a flat surface due to attritious wear, possibly because the diamond has been macro-fractured and was not in contact with the grinding wheel.
- *Particle diamond* #2: A large wear flat area can be seen on the top half of particle diamond #2, as shown in Fig. 11(c). The close-up views in Fig. 11(d) and (e) show the flat area and the ridge-shaped fracture surface of the diamond.
- *Particle diamond* #3: The whole surface of diamond particle #3 is worn flat. This shining wear surface, along with the wear surface in particle diamond #2, can be seen visually. This diamond particle was carrying a large contact or truing force. The erosion of the metal bond on the right side of the particle diamond can be seen in Fig. 11(f). Fig. 11(g) shows the edge of the wear flat surface of the diamond.
- *Diamond pulled-out*: Two cavities created by pulled-out diamond particles can be seen in Fig. 9(b) between diamond particles #2 and #3.
- *Particle diamonds* #4 *and* #5: Fig. 9(b) shows that the particle diamonds #4 and #5 were just exposed and have not yet engaged grinding wheel. Figs. 11(h)–(k) illustrate the erosion on the surface of particle diamond #4 and #5, respectively. The close-up view of these particles are shown in Fig. 10(i), (j), and (l).

5. Grinding forces

The grinding wheel after truing is used for cylindrical grinding of a zirconia ceramic workpiece. The grinding spindle power change during grinding was recorded and

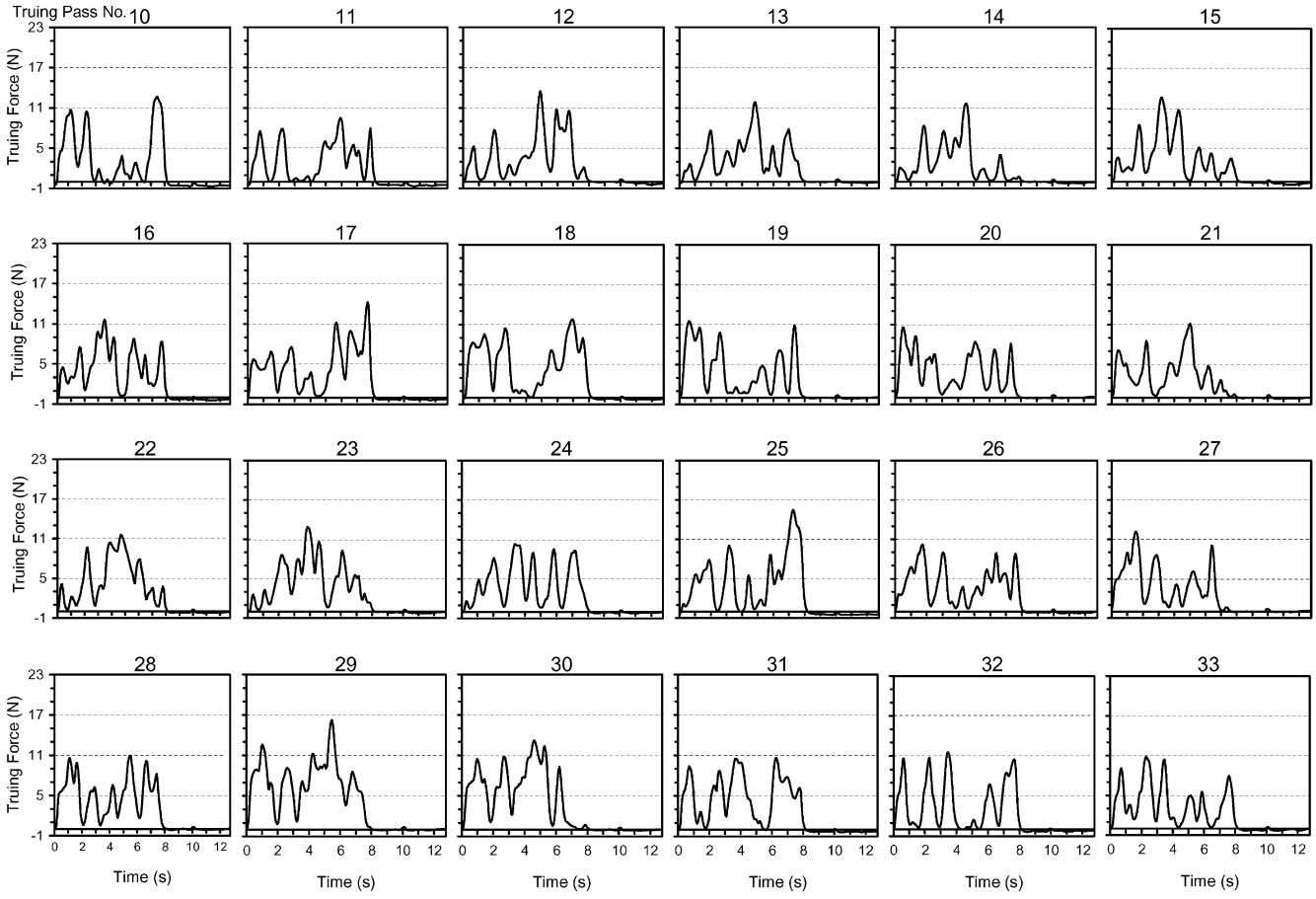

Fig. 8. Twenty-four consecutive tangential truing force data for truing at 13 μm feed and 125 mm/min traverse speed using the particle diamond blade tool.

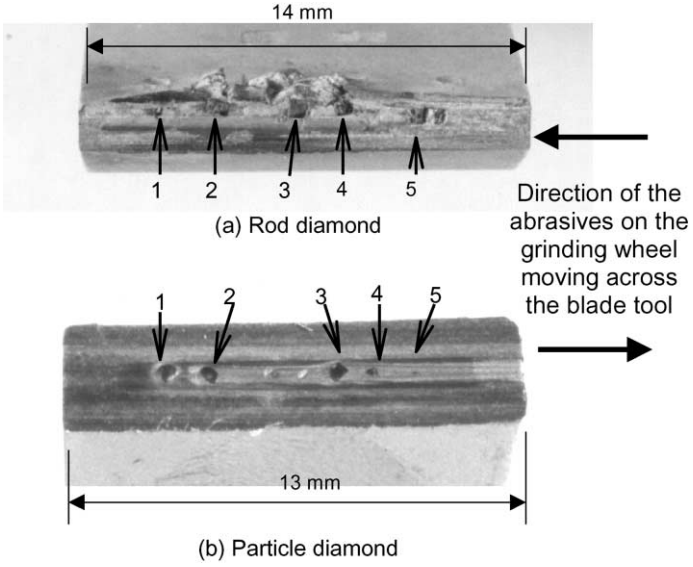

Fig. 9. Pictures of the worn surface of two blade diamond tools.

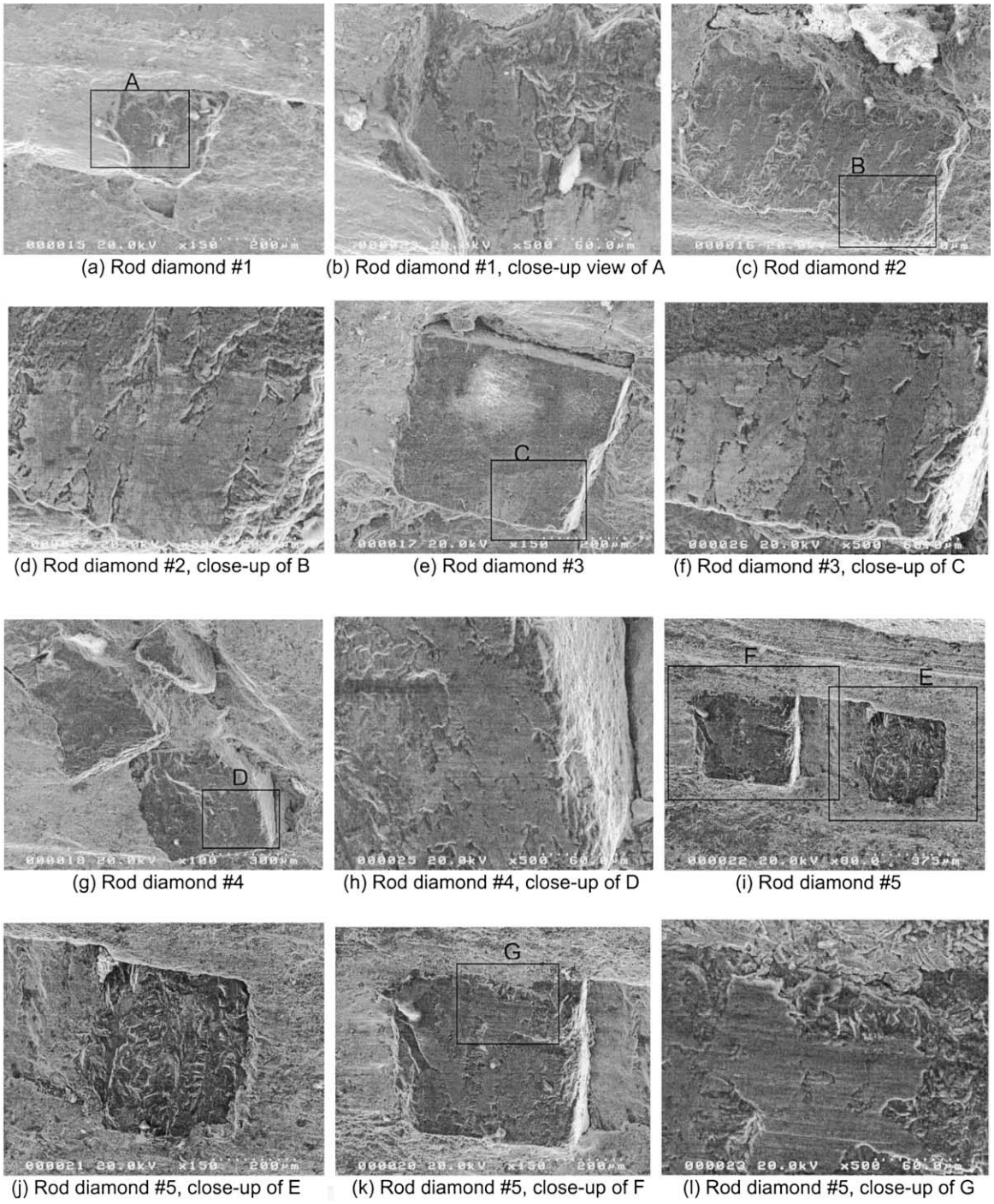

Fig. 10. SEM micrographs of five rod diamonds on the blade tool.

converted to the specific tangential grinding force. The results are shown in Fig. 12.

The same grinding wheel trued by rod diamond exhibit higher grinding force. Truing studies has reported that a dull diamond tool with large flat wear surface, or high overlap ratio in truing terminology, will generate a grinding wheel surface topology, which exhibits larger forces during grinding and generates finer surface finish on the ground workpiece [9–11]. Fig. 11 indicates the possibly that the higher grinding force for rod diamond trued wheel is due to the larger surface contact area or higher overlap ratio of the rod diamond tool. The effect of truing feed and traverse speed on the grinding force was not obvious.

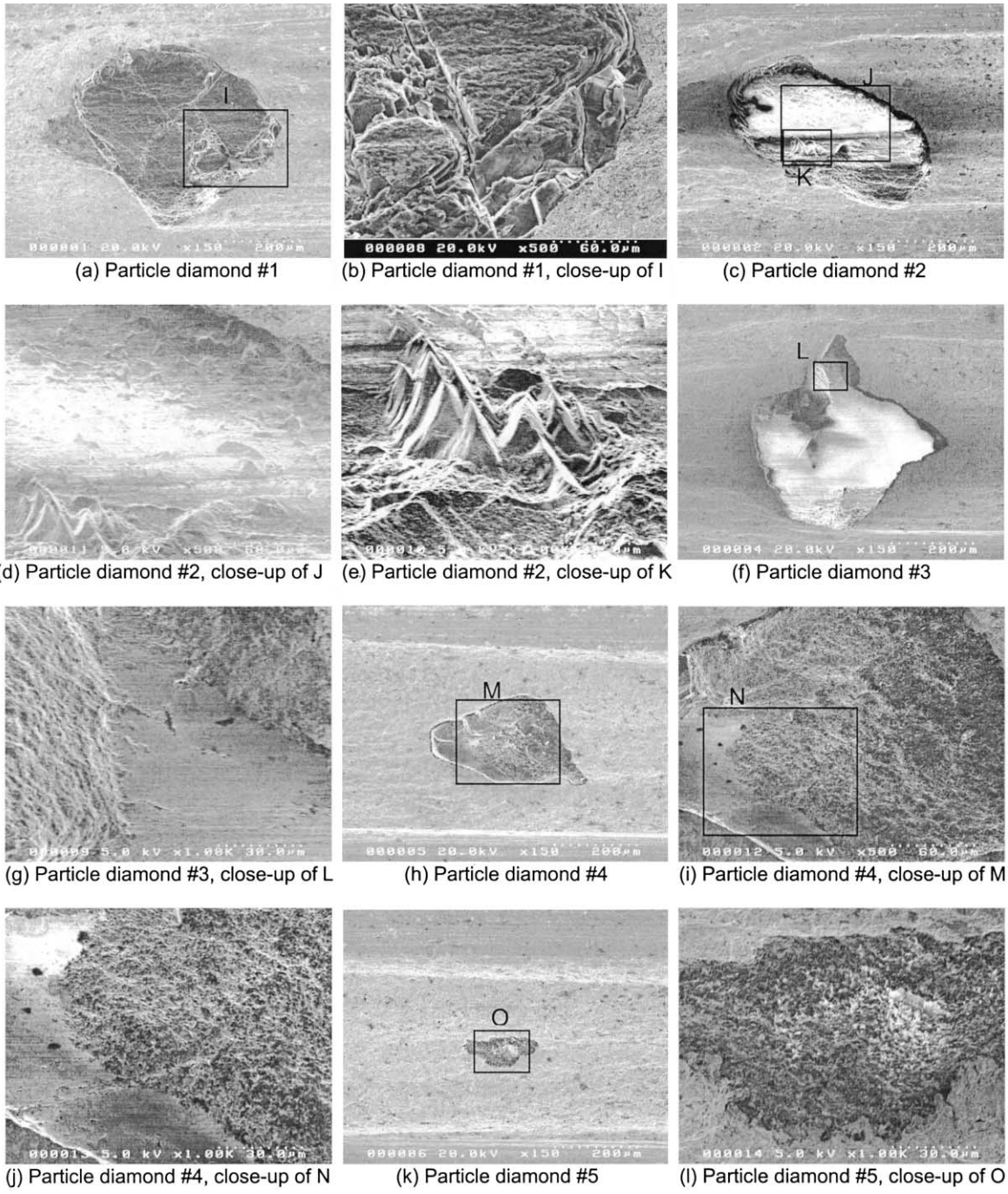

(a) Particle diamond #1 (b) Particle diamond #1, close-up of I (c) Particle diamond #2

(d) Particle diamond #2, close-up of J (e) Particle diamond #2, close-up of K (f) Particle diamond #3

(g) Particle diamond #3, close-up of L (h) Particle diamond #4 (i) Particle diamond #4, close-up of M

(j) Particle diamond #4, close-up of N (k) Particle diamond #5 (l) Particle diamond #5, close-up of O

Fig. 11. SEM micrographs of five particle diamonds on the blade tool.

6. Concluding remarks

The measurement of grinding spindle power change using a power sensor and the calculation of tangential truing and grinding forces were presented. A signal processing procedure was developed to analyze the truing force data statistically. SEM was used to examine the wear of rod and particle diamond blade tools. The micro- and macro-fracturing of the diamond were identified from both the truing force data and SEM micrographs.

For an ideal blade diamond tool, the macro-fracture of the diamond particle or rod should be minimized. This can be accomplished by tailoring the blade diamond tool for a specific application. The truing process monitoring system used in this study can be a helpful aid to select a suitable blade diamond tool for precision form generation of the grinding wheel.

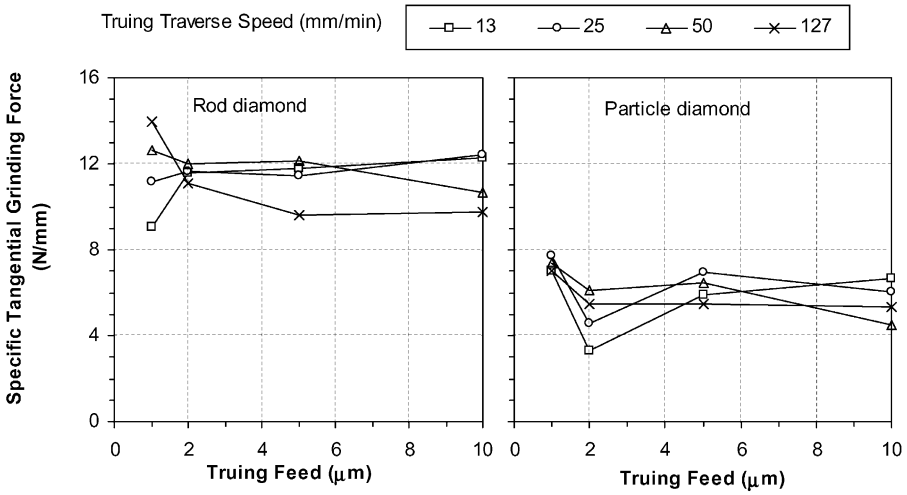

Fig. 12. Peak specific tangential grinding force for the wheel trued by rod and particle diamond tools.

Acknowledgements

Portion of this research was sponsored by the National Science Foundation Grant #9983582 and the REU supplement (Dr. K.P. Rajurkar, Program Director).

References

[1] S.W. Webb, W.E. Jackson, J. Manufact. Sci. Eng. 120 (1998) 84–92.
[2] Y.S. Liao, S.Y. Luo, Wear 157 (1992) 325–337.
[3] S.Y. Luo, Int. J. Mach. Tools Manufact. 36 (1996) 661–672.
[4] D.N. Wright, H. Wapler, Ann. CIRP 35 (1986) 239–244.
[5] D. Miller, A. Ball, Wear 141 (1991) 311–320.
[6] F.G. Werner, E. Minke, in: Proceedings of 11th North American Manufacturing Research Conference, Society of Manufacturing Engineers, 1983, pp. 11–17.
[7] J.A. Williams, Engineering Tribology, Oxford University Press, Oxford, 1994, 179 pp.
[8] A.J. Shih, Mach. Sci. Technol. 2 (1998) 13–28.
[9] A.J. Shih, Int. J. Mach. Tools Manufact. 40 (2000) 1755–1774.
[10] F. Klocke, W. Koenig, Ann. CIRP 44 (1995) 305.
[11] C.E. Davis, Int. J. Mach. Tool Des. Res. 14 (1973) 33–52.